PAPER • OPEN ACCESS

Time-energy filtering of single electrons in ballistic waveguides

View the article online for updates and enhancements.

New Journal of Physics

The open access journal at the forefront of physics

PAPER

CrossMark

Time-energy filtering of single electrons in ballistic waveguides

Elina Locane[1], Piet W Brouwer[1] and Vyacheslavs Kashcheyevs[2]

[1] Dahlem Center for Complex Quantum Systems and Institut für Theoretische Physik, Freie Universität Berlin, Arnimallee 14, D-14195 Berlin, Germany
[2] Department of Physics, University of Latvia, Jelgavas street 3, LV-1004 Riga, Latvia

E-mail: slava@latnet.lv

Abstract

Characterizing distinct electron wave packets is a basic task for solid-state electron quantum optics with applications in quantum metrology and sensing. A important circuit element for this task is a non-stationary potential barrier that enables backscattering of chiral particles depending on their energy and time of arrival. Here we solve the quantum mechanical problem of single-particle scattering by a ballistic constriction in an fully depleted quantum Hall system under spatially uniform but time-dependent electrostatic potential modulation. The result describes electrons distributed in time-energy space according to a modified Wigner quasiprobability distribution and scattered with an energy-dependent transmission probability that characterizes constriction in the absence of modulation. Modification of the incoming Wigner distribution due to external time-dependent potential simplifies in case of linear time-dependence and admits semiclassical interpretation. Our results support a recently proposed and implemented method for measuring time and energy distribution of solitary electrons as a quantum tomography technique, and offer new paths for experimental exploration of on-demand sources of coherent electrons.

1. Introduction

Electron quantum optics is a relatively new field, aiming to reproduce quantum optics experiments with electron wave packets instead of photons [1–4]. It offers the prospects of probing the interaction between just a few electrons, as well as studying phenomena on the scale of electron coherence time. The field has potentially promising applications in signal processing [5] and quantum sensing [6].

One of the crucial ingredients that has made the investigation of single electron excitations in ballistic waveguides possible is the advent of devices that emit ordered streams of electrons with sufficient separation between individual particles [7–21]. Techniques to characterize quantum properties of electrical current have been adapted from photon quantum optics. Statistical properties of the source and the exchange statistics of the particles can be probed using intensity interferometers such as the Hanbury–Brown–Twiss and Hong–Ou–Mandel interferometers [22–27], while coherence, entanglement, and the wave-like nature of particles can be probed using amplitude interferometers such as the Mach–Zehnder interferometer [28–30].

However, most of the existing electron quantum optics experiments have focused on single-electron sources that emit electrons close to the Fermi sea [3, 31]. These excitations can be accessed by perturbing the Fermi sea through the application of periodic gate potentials allowing for quantum state reconstruction through correlation measurements between the unknown and the reference signal [32–34]. Such an approach is not possible in the case of 'high-energy' electrons [19, 35–39] emitted far above (tens of meV) the Fermi sea, because they do not overlap with perturbations around the Fermi energy. These excitations provide a new kind of quasi-particle whose coherence properties are largely unexplored.

A recent work by Fletcher *et al* [40] addresses the characterization of these 'high-energy' electrons by using an energy barrier that is tuned to match the energy of the quasiparticles. The authors propose and implement an electron tomography protocol that reconstructs the joint energy-time quasi-probability distribution $p(E, t)$ of
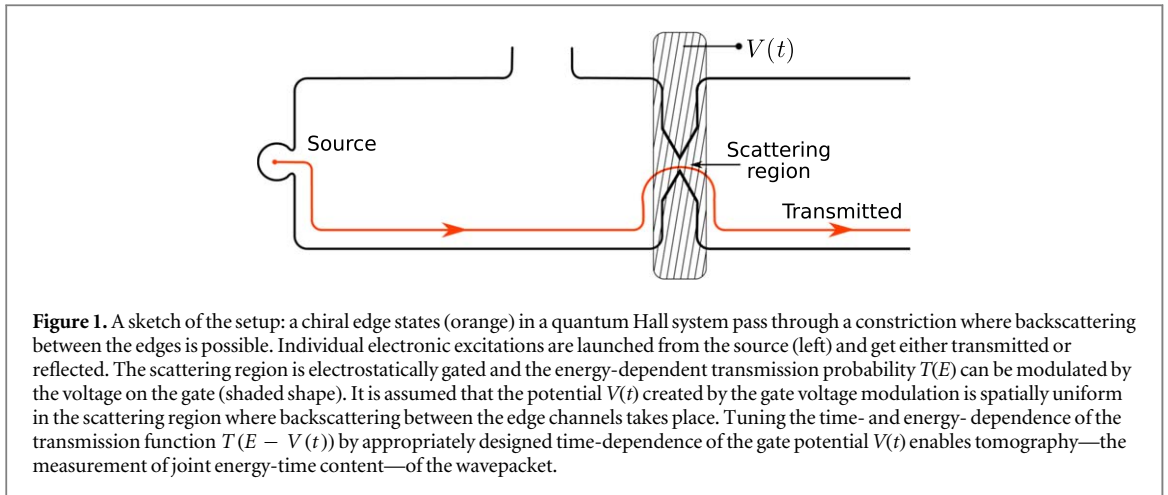
Figure 1. A sketch of the setup: a chiral edge states (orange) in a quantum Hall system pass through a constriction where backscattering between the edges is possible. Individual electronic excitations are launched from the source (left) and get either transmitted or reflected. The scattering region is electrostatically gated and the energy-dependent transmission probability $T(E)$ can be modulated by the voltage on the gate (shaded shape). It is assumed that the potential $V(t)$ created by the gate voltage modulation is spatially uniform in the scattering region where backscattering between the edge channels takes place. Tuning the time- and energy- dependence of the transmission function $T(E - V(t))$ by appropriately designed time-dependence of the gate potential $V(t)$ enables tomography—the measurement of joint energy-time content—of the wavepacket.

the incoming electrons by measuring the transmitted charge through an energy barrier whose height is varied linearly in time. The experimental setup can be described by a model shown schematically in figure 1, where the time-dependent energy barrier is modelled with a static constriction subject to a (locally) uniform gate voltage $V(t) = V_0 + \alpha t$. The two parameters of the linear modulation (the offset in energy V_0 and the slope α in the time-energy plane) provide a two-dimensional map of the charge $Q(V_0, \alpha)$, that is used to infer $p(E, t)$ using inversion techniques from tomographic image processing [40]. The key relation connecting the properties of the incoming wave-packets with the measured signal can be written as

$$Q = e \int dE \, dt \, T(E) \, p(E + V(t), t), \tag{1}$$

where $T(E)$ is the energy-dependent transmission probability of the constriction in the absence of the gate voltage modulation.[3]

Equation (1) has been previously derived classically [39] by considering scattering of a statistical ensemble of electrons with simultaneously well-defined energy and time of arrival, impinging on a scattering barrier with a transmission probability $T(E, t)$. Due to gauge invariance under uniform modulation, shift in voltage is equivalent to shift in energy, $T(E, t) = T(E - V(t), t)$, giving equation (1). In this classical picture $p(E, t)$ is simply the joint probability density characterizing the electrons emitted by the source.
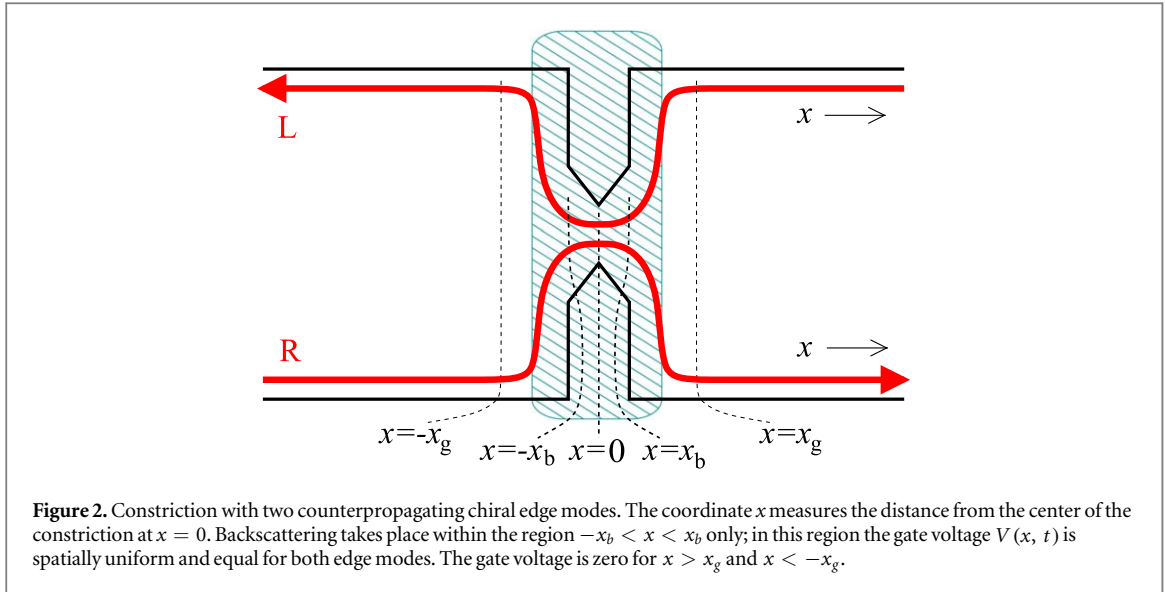
In this work, we derive a general expression for the transmitted charge for an arbitrary time-dependence of $V(t)$ and show that the distribution $p(E, t)$ in a general case needs to be replaced by a suitably modified Wigner function. We also show that if the gate voltage $V(t)$ has a linear dependence on time, no modification of the Wigner function is necessary and equation (1) is valid if we take $p(E, t)$ to be the Wigner function of the incoming electron $\rho_{\mathrm{in}}(E, t)$. This confirms that the protocol implemented in [40] can be used not only for classical but also for quantum tomography, i.e. quantum state reconstruction. We argue that if there are deviations from a linear time dependence of the gate potential, the modified Wigner function instead of the actual incoming Wigner function will be observed. We note that the Wigner distribution function has previously been found to be a useful concept in electron quantum optics [33, 41, 42]. Here it appears naturally as a quantum counterpart of the classical probability density.

Our manuscript is organized as follows: In section 2 we give a precise definition of our system and of the approximations involved, as well as introduce the Wigner distribution function. Our main result, a quantum version of equation (1), is presented and derived in section 3. In that section we also discuss special cases, such as a gate voltage with a linear time dependence (for which equation (1) is exact), a gate voltage with sharp edges, and the limit of a slowly varying gate voltage. Section 4 illustrates our results, by comparing the 'classical' and 'quantum' expressions for a few characteristic examples. In section 6 we discuss the implication of our results for the analysis and improvement of electron tomography experiments. We conclude in section 7.

2. Model

We consider a constriction with two counterpropagating quantum Hall edge channels. The coordinate x measures the distance along the edge, taking the center of the constriction as the origin, such that points to the left (right) of the constriction have negative (positive) x, see figure 2. The Hamiltonian for the two

---

[3] Strictly speaking, in equation (1) $V(t)$ should be replaced by the integral of the electric field for electrons traveling along the edge, which need not be equal to $V(t)$ for a time-dependent gate potential, see section 3.

Figure 2. Constriction with two counterpropagating chiral edge modes. The coordinate x measures the distance from the center of the constriction at $x = 0$. Backscattering takes place within the region $-x_b < x < x_b$ only; in this region the gate voltage $V(x, t)$ is spatially uniform and equal for both edge modes. The gate voltage is zero for $x > x_g$ and $x < -x_g$.

counterpropagating edge states reads

$$\hat{H} = -\mathrm{i}\hbar v \hat{\sigma}_3 \frac{\partial}{\partial x} + \hat{H}_{\mathrm{bs}} + \hat{V}(x, t), \tag{2}$$

where v is the electron velocity, $\hat{\sigma}_3$ is the Pauli matrix, and the 2×2 matrix structure refers to the two edges. The second term $\hat{H}_{\mathrm{bs}}$ describes backscattering in the constriction, and

$$\hat{V}(x, t) = \begin{pmatrix} V_{\mathrm{R}}(x, t) & 0 \\ 0 & V_{\mathrm{L}}(x, t) \end{pmatrix} \tag{3}$$

is a gate potential. The backscattering Hamiltonian H_{bs} is characterized by its transmission probability

$$T(E) = |\tau(E)|^2, \tag{4}$$

in the absence of the gate voltage $V(x, t)$, where $\tau(E)$ is the transmission amplitude.

Since backscattering takes place locally at the contact, the backscattering term has finite support which we define to be $|x| < x_b$. Outside of the constriction ($|x| > x_b$), the tunnelling amplitude between the left movers and the right movers is exponentially suppressed due to the Lorentz-force induced localization of the edge states at the opposite sides of the Hall system. This makes x_b a well-defined quantity despite the non-locality of tunneling in general.

We furthermore assume that the externally controlled part of the potential is spatially uniform inside the backscattering region:

$$V_{\mathrm{R}}(x, t) = V_{\mathrm{L}}(x, t) = V(t) \text{ for } |x| < x_b. \tag{5}$$

For a point-contact geometry sketched in figure 2, this approximation is justified because the two counterpropagating edge states are closest in centre of the constriction where the effect of a sufficiently wide top gate (shaded region) is spatially uniform. Although, strictly speaking, the condition (5) is stronger than the assumption that a (time-independent) shift of the gate voltage V is equivalent to a shift in energy, the relation $T(E, V) = T(E - V)$ (which is central to the tomography experiment [40]) does not hold for a generic scatterer if the condition (5) is not satisfied.

Finally, we set the gate potential to zero sufficiently far away from the constriction,

$$V_{\mathrm{R}}(x, t) = V_{\mathrm{L}}(x, t) = 0 \text{ for } |x| > x_g. \tag{6}$$

We consider a wavepacket incident on the constriction, such that it reaches the center of the constriction for $t \approx 0$. For times $t \to -\infty$ this initial state is described by the wavefunction

$$\psi_{\mathrm{in}}(x, t) = \varphi_{\mathrm{in}}(t - x/v) \begin{pmatrix} 1 \\ 0 \end{pmatrix}, \tag{7}$$

where the function $\varphi_{\mathrm{in}}(t)$ is peaked near $t = 0$. The initial-state wavefunction is normalized such that

$$\int_{-\infty}^{\infty} \mathrm{d}t \, |\varphi_{\mathrm{in}}(t)|^2 = 1. \tag{8}$$

Similarly, for times $t \rightarrow \infty$ the wavepacket is described by the wavefunction

$$\psi_{\text{out}}(x, t) = \begin{pmatrix} \varphi_{\text{out}}(t - x/v) \\ \varphi'_{\text{out}}(t + x/v) \end{pmatrix}, \tag{9}$$

where $\varphi_{\text{out}}(t - x/v)$ represents the transmitted part of the wave packet, and $\varphi'_{\text{out}}(t + x/v)$ represents the reflected part.

Instead of the function $\varphi_{\text{in}}(t)$ it is convenient to use the Wigner transform $\rho_{\text{in}}(E, t)$, which is defined as

$$\rho_{\text{in}}(E, t) = \frac{1}{\pi \hbar} \int_{-\infty}^{+\infty} \mathrm{d}t' \mathrm{e}^{2\mathrm{i}Et'/\hbar} \varphi_{\text{in}}^*(t - t') \varphi_{\text{in}}(t + t'). \tag{10}$$

The classical limit of the Wigner distribution function $\rho(E, t)$ is the joint probability density $p(E, t)$ of energy E and time t and corresponds to a Dirac delta distribution peaked around the classical trajectory $E(t)$. Correspondingly, the spread of the Wigner distribution around the classical trajectory is a manifestation of the quantumness of the wave packet [42]. The interpretation of $\rho(E, t)$ as a joint probability distribution is not rigorous, though, since the Wigner distribution can also take on negative values. Integrating $\rho(E, t)$ with respect to one of its arguments, however, one obtains a positive function, which is the probability density (marginal distribution) of the other argument, i.e.

$$p_E(E) = \int_{-\infty}^{+\infty} \rho(E, t) \, \mathrm{d}t,$$

$$p_t(t) = \int_{-\infty}^{+\infty} \rho(E, t) \, \mathrm{d}E. \tag{11}$$

3. Transmitted charge

3.1. Derivation of the main result
We now proceed with the calculation of the charge Q transmitted through the constriction,

$$Q = e \int \mathrm{d}t \, |\varphi_{\text{out}}(t)|^2. \tag{12}$$

For this calculation it is sufficient to consider the right-moving edge only. We drop the spinor notation of the previous section, use the scalar wavefunction $\psi(x, t)$ to refer to the wavefunction component at the right-moving edge, and write $V(x, t)$ instead of $V_{\text{R}}(x, t)$.

In the absence of the gate voltage, $V(x, t) = 0$, the result can be easily expressed in terms of the energy-dependent transmission probability $T(E)$,

$$Q = e \int \mathrm{d}E \, \mathrm{d}t \, T(E) \, \rho_{\text{in}}(E, t), \tag{13}$$

which is a special case of the classical equation (1), with $p(E, t)$ replaced by $\rho_{\text{in}}(E, t)$.

We now consider the general case of time- and energy-dependent scattering, specializing to the geometry described in section 2, for which the time dependence comes from the gate potential $V(x, t)$.

Since the potential $V(x, t) = 0$ for $x < -x_g$, the initial-state solution (7) is valid for all $x < -x_g$. Similarly, the expression (9) for the transmitted wavepacket is valid for all $x > x_g$. In the first step of our calculation we solve the time-dependent Schrödinger equation to calculate the wavefunction at all positions $x \leqslant -x_b$ and $x \geqslant x_b$,

$$\psi(x, t) = \varphi_{\text{in}}(t - x/v) \, \mathrm{e}^{-\frac{\mathrm{i}}{\hbar} \int_{-\infty}^{t} \mathrm{d}t' V[x - v(t-t'), t']}, \quad x \leqslant -x_b,$$

$$\psi(x, t) = \varphi_{\text{out}}(t - x/v) \, \mathrm{e}^{+\frac{\mathrm{i}}{\hbar} \int_{t}^{\infty} \mathrm{d}t' V[x - v(t-t'), t']}, \quad x \geqslant x_b. \tag{14}$$

In a second step we perform the gauge transformation

$$\widetilde{\psi}(x, t) = \psi(x, t) \, \mathrm{e}^{\frac{\mathrm{i}}{\hbar} \int_{-\infty}^{t} V(t') \, \mathrm{d}t'}, \tag{15}$$

where $V(t)$ is the value of the gate voltage at the center of the constriction, see equation (5). For $-x_b < x < x_b$ the transformed wavefunction $\widetilde{\psi}$ satisfies a Schrödinger equation without gate potential, so that

$$\widetilde{\psi}(x_b, t + x_b/v) = \int \tau(t - t') \, \widetilde{\psi}(-x_b, t' - x_b/v) \, \mathrm{d}t', \tag{16}$$

where

$$\tau(t) = \frac{1}{2\pi\hbar} \int dE \ e^{-iEt/\hbar} \ \tau(E) \tag{17}$$

is the Fourier transform of the constriction's transmission amplitude $\tau(E)$. The choice of the offsets in the time arguments in equation (16) ensures that, for a perfectly transmitting constriction with $\tau(t) = \delta(t)$, $\widetilde{\psi}(x, t)$ is a function of $t - x/v$ only.

Note that we do not need to invoke $\psi(x, t)$ explicitly for $x \in [-x_b, +x_b]$—all the information about coherent dynamics inside the modulated scattering region is encoded in the matrix element $\tau(t)$ of the time evolution operator which is time-translation invariant in the gauge expressed by equation (15). This is valid as long as the modulation is spatially flat as expressed by condition (5). Matching equations (14) and (16) at $x = -x_b$ and $x = +x_b$, we find

$$\varphi_{\text{out}}(t) = \int dt' \ \tilde{\tau}(t, t') \ \varphi_{\text{in}}(t'), \tag{18}$$

with

$$\tilde{\tau}(t, t') = e^{-\frac{i}{\hbar}\int_{-\infty}^{t'} dt'' V[-v(t'-t''),t''] - \frac{i}{\hbar}\int_{t'}^{t} dt'' V(t'')}$$
$$\times e^{-\frac{i}{\hbar}\int_{t}^{\infty} dt'' V[-v(t-t''),t'']} \tau(t - t'). \tag{19}$$

Transmitted charge (12) can be written in the form that closely resembles the classical result (1) and the limiting case (13),

$$Q = e \int dt \ dE \ T(E) \ \tilde{\rho}(E, t), \tag{20}$$

but with the function

$$\tilde{\rho}(E, t) = \frac{1}{\pi\hbar} \int dt' \varphi_{\text{in}}(t + t') \varphi_{\text{in}}^*(t - t') \ e^{\frac{i}{\hbar}\int_{t-t'}^{t+t'} dt_1[E+\mathcal{V}(t_1)]} \tag{21}$$

instead of $p(E + V(t), t)$. Here

$$\mathcal{V}(t) = \int_{-\infty}^{0} dx \left(\frac{\partial V(x, t')}{\partial x}\right)_{t' \to t+x/v} \tag{22}$$

is the integral of the electric field along the electron's trajectory. The expressions (20)–(22) are the key results of this article.

The modified Wigner function $\tilde{\rho}(E, t)$ can be interpreted as the Wigner representation (10) of a modified incoming asymptotic state, $\tilde{\varphi}_{\text{in}}(t) = \varphi_{\text{in}}(t) \ e^{-i\int^t \mathcal{V}(t')dt'/\hbar}$. The effective gate potential $\mathcal{V}(t)$ represents the relevant modification of the applied gate potential $V(t)$ due to finite spatial extent of the gate. Although $\tilde{\varphi}_{\text{in}}(t)$, and hence $\tilde{\rho}(E, t)$, does not in general represent the actual quantum state of the electron at any time instant, $\tilde{\rho}(E, t)$ can still be measured as the outcome of a tomographic reconstruction, as we argue in section 6.

The main result (20) can easily be generalized to the case in which the incoming state is not a pure state. In this case the Wigner function is defined with the help of the single-particle density matrix $\hat{\rho}$ and the product $\varphi_{\text{in}}^*(t - t')\varphi_{\text{in}}(t + t')$ in equation (20) is replaced by the matrix element $\langle t - t'|\hat{\rho}|t + t'\rangle$.

Our model Hamiltonian (2) does not take into account decoherence during the propagation along the chiral edge, or dispersion resulting from (small) corrections to the linear kinetic energy term. Dispersion preserves the pure-state character of the incoming wavepacket, whereas decoherence changes it into a mixed state, which must be described using a density matrix (see the preceding remark). If these processes are relevant (e.g. due to phonon emission [43]), the modified Wigner function in equation (21) must be calculated with respect to the Wigner function of the wavepacket as it arrives at the constriction, i.e. it should include the decoherence and dispersion effects accumulated during the propagation along the chiral edge. Dispersion or decoherence processes associated with the (short) propagation inside the constriction region (i.e. for $-x_g < x < -x_b$) are not included in our approach. These can, however, be assumed to be small, since the size of the constriction itself is typically much less than the distance between the source and the constriction.

3.2. Special cases
Below we consider a number of special cases of $V(x, t)$ and discuss the corresponding forms of $\mathcal{V}(t)$ and $\tilde{\rho}(E, t)$.

3.2.1. Time-independent potential
One verifies that for a time-independent potential $\partial V(x, t)/\partial t = 0$ we have $\mathcal{V}(t) = V$ and

$$\tilde{\rho}(E, t) = \rho_{\text{in}}(E + V, t), \tag{23}$$

where V is the value of the spatially uniform potential in the scattering region. We see that the time-independent V just changes the energy reference level in equation (13), as expected from gauge invariance.

3.2.2. Factorized time and coordinate dependence
If the time and coordinate dependence is such that $V(x, t) = u(x) V(t)$ where the shape function $u(x)$ satisfies

$$u(x) = \begin{cases} 1, & -x_g < x < +x_g, \\ 0, & x < -x_b \text{ or } x > +x_b \end{cases} \tag{24}$$

then

$$\mathcal{V}(t) = \int_{-x_g}^{-x_b} \mathrm{d}x \; V(t + x/v) \, \frac{\mathrm{d}u}{\mathrm{d}x}. \tag{25}$$

Typically, $u(x)$ is expected to be a smooth sigmoid function, in which case the convolution (25) limits the sharpness of time-dependent features in $\mathcal{V}(t)$ compared to $V(t)$.

3.2.3. Gate potential with sharp edges
In the limit of a sharp edge, $-x_g \rightarrow -x_b$, equation (25) with $\mathrm{d}u/\mathrm{d}x \rightarrow \delta(x + x_g)$ is applicable, and the correction of $V(t)$ becomes just the shift of the argument,

$$\mathcal{V}(t) = V(t - x_g/v). \tag{26}$$

We see that the modification of the wave-packet happens at the edge of the gate-affected region.

3.2.4. Linear time dependence
The experiment of [40] features a potential with a linear time dependence,

$$V(x, t) = V_0(x) + t \, V_1(x), \tag{27}$$

which yields a linear $\mathcal{V}(t)$,

$$\mathcal{V}(t) = V_0(0) - \frac{1}{v} \int_{-\infty}^{0} \mathrm{d}x \; V_1(x) + V_1(0) \, t. \tag{28}$$

In this case we find that the function $\tilde{\rho}(E, t)$ can be expressed directly in terms of the Wigner distribution $\rho_{\text{in}}(E, t)$ of the incoming wavepacket,

$$\tilde{\rho}(E, t) = \rho_{\text{in}}[E + \mathcal{V}(t), t]. \tag{29}$$

Upon comparing equations (20) and (29) with (1) we conclude that for a potential with linear time dependence the quantum-mechanical theory reproduces the classical approximation (1).

Note that $\mathcal{V}(t)$ is not in general equal to the value of the potential $V(x = 0, t) = V(t)$ at the centre of the gate at the same time instant t, but rather at an earlier time corresponding to the effective position of the gate edge. We can define the latter explicitly by rewriting equation (28) as $\mathcal{V}(t) = V(t + \tilde{x}_g/v) = V_0(0) + V_1(0)(t + \tilde{x}_g/v)$ where $\tilde{x}_g < 0$ is the center of mass of the accelerating electric field distribution, $\tilde{x}_g = \int_{-\infty}^{0} x \, (\mathrm{d}V_1/\mathrm{d}x) \, \mathrm{d}x \, / V_1(0)$. For a sharp edge, we have $\tilde{x}_g = -x_g$, in accord with equation (26).

3.2.5. Slowly varying potential
If the rate of change of the gate voltage is slow compared to the velocity of the wave packet, it is reasonable to expand

$$V(x, t) = V_0(x) + V_1(x)t + \frac{1}{2}V_2(x)t^2 + \ldots. \tag{30}$$

Truncating after the quadratic term, this leads to the formal expression

$$\tilde{\rho}(E, t) = \mathrm{e}^{-\frac{1}{24}V_2(0)\hbar^2 \frac{\partial^3}{\partial E^3}}\rho_{\text{in}}[E + \mathcal{V}(t), t], \tag{31}$$

where

$$\mathcal{V}(t) = \int_{-\infty}^{0} dx \left(\frac{\partial V(x, t')}{\partial x} \right)_{t' \to t + x/v} = V_0(0) - \int_{-\infty}^{0} dx \left[\frac{V_1(x)}{v} + \frac{V_2(x)x}{v^2} \right] + \left(V_1(0) - \int_{-\infty}^{0} dx \frac{V_2(x)}{v} \right) t + \frac{1}{2} V_2(0) t^2.$$
(32)

Equation (31) contains the result (29) for a gate potential with a linear time dependence and is a good starting point for an expansion in a small second derivative $V_2(x)$ of the time-dependent gate potential.

3.2.6. Linear time dependence superimposed on an arbitrary gate potential $V'(x, t)$
If on top of a linear time dependence the potential $V(x, t)$ also contains arbitrary additional terms $V'(x, t)$,

$$V(x, t) = V_0(x) + tV_1(x) + V'(x, t),$$
(33)

the modified Wigner function $\tilde{\rho}(E, t)$ can be expressed as

$$\tilde{\rho}(E, t) = \tilde{\rho}'(E + \mathcal{V}(t), t),$$
(34)

where $\mathcal{V}(t)$ is given by equation (28) and $\tilde{\rho}'(E + \mathcal{V}(t), t)$ is calculated with respect to $V'(x, t)$ only. The relevance of this result will be discussed in section 6. (Note that equation (34) simplifies to equation (29) for the special case $V'(x, t) = 0$.)

4. Examples

In this section we show explicit results for three examples: a gate voltage with linear time dependence, a gate voltage with an abrupt step-like time dependence, and a gate voltage with parabolic time dependence. We take the spatial profile of the gate voltage $V(x, t)$ to be a spatially uniform potential with sharp edges at $x = \pm x_g$. We also shift the time origin by $-x_b/v$, so that the integral $\mathcal{V}(t)$ of the electric field can be replaced directly by the potential $V(t)$ at the center of the constriction, see equation (26). For the incoming wavepacket we take the uncorrelated Gaussian form,

$$\varphi_{\text{in}}(t) = \frac{1}{(2\pi\sigma_t^2)^{1/4}} e^{-\frac{iE_0 t}{\hbar} - \frac{t^2}{4\sigma_t^2}}.$$
(35)

The scale σ_t sets the characteristic width in the time domain. The energy of the wavepacket is centered around E_0, with fluctuations of order $\hbar/\sigma_t$. The Wigner distribution $\rho_{\text{in}}(E, t)$ corresponding to the wavefunction (35) is

$$\rho_{\text{in}}(E, t) = \frac{1}{\pi\hbar} e^{-2(E-E_0)^2\sigma_t^2/\hbar^2 - t^2/(2\sigma_t^2)}.$$
(36)

For the examples in this and the following sections, we model the energy-dependence of the transmission probability through a static constriction as

$$T(E) = \frac{1}{2} \left[1 + \text{erf}\left(\frac{E}{\delta\sqrt{2}} \right) \right],$$
(37)

where δ gives the width of the energy window in which the transmission changes from 0 to 1 and the zero of energy is chosen to coincide with half-transmission point of the constriction. For the numerical calculations we will take the idealized limit $\delta \to 0$, corresponding to a point contact that perfectly selects the sign of the electron's energy.

4.1. Linear ramp
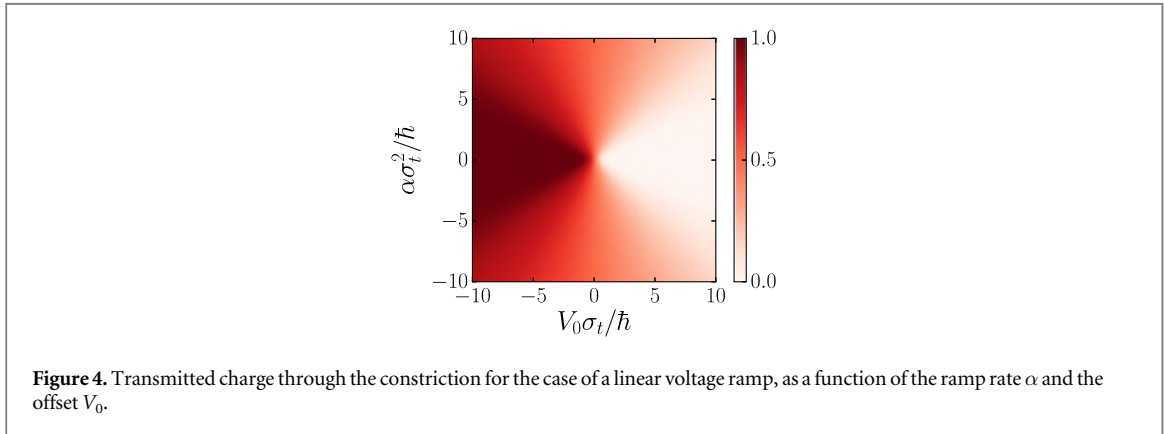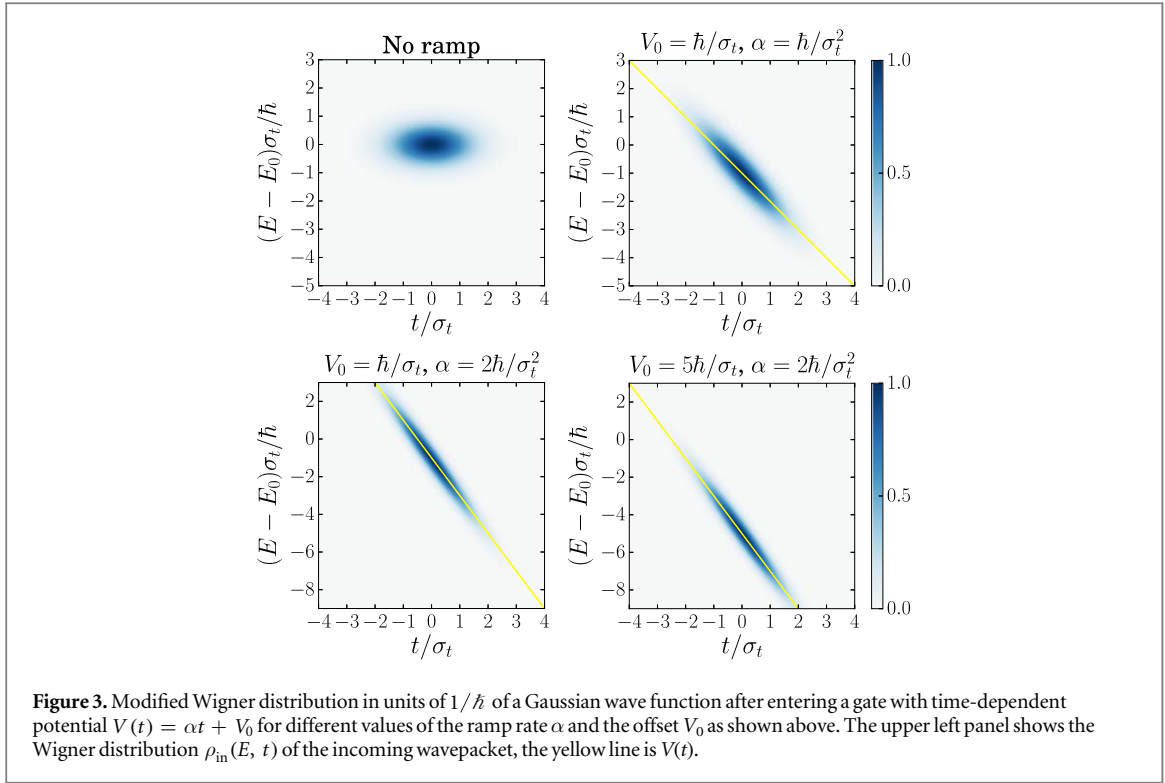We first consider the case of a gate voltage with a linear time dependence,

$$V(t) = \alpha t + V_0.$$
(38)

Gate voltages with different offsets V_0 are related by a delay time $t_d = -V_0/\alpha$. For this case the modification of the Wigner distribution can be obtained from equation (29), which gives:

$$\tilde{\rho}(E, t) = \frac{1}{\pi\hbar} e^{-2(E-E_0+V(t))^2\sigma_t^2/\hbar^2 - t^2/2\sigma_t^2}.$$
(39)

The modified Wigner distribution for different values of the ramp rate α and the offset V_0 is shown in figure 3, along with the non-transformed Wigner distribution. In comparison to the original Wigner distribution ρ_{in}, the modified distribution $\tilde{\rho}$ has a shifted center energy, determined by the offset V_0, and it is stretched along a straight line with slope $-\alpha$. Figure 4 shows the transmitted charge as a density plot in the case of a linear ramp as a function of the parameters α and V_0. This transformation gives the basis for interpreting $p(E, t)$ in equation (1) as the $\rho_{\text{in}}(E, t)$, as discussed in the discussed in section 3.
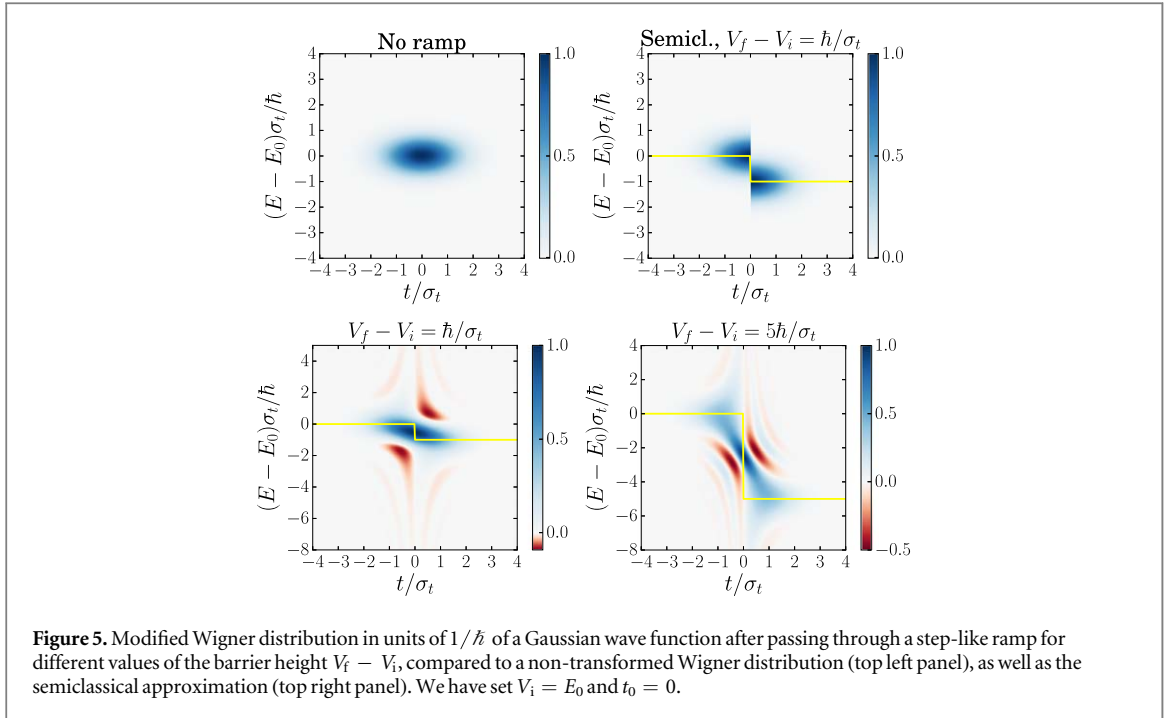
Figure 3. Modified Wigner distribution in units of $1/\hbar$ of a Gaussian wave function after entering a gate with time-dependent potential $V(t) = \alpha t + V_0$ for different values of the ramp rate α and the offset V_0 as shown above. The upper left panel shows the Wigner distribution $\rho_{in}(E, t)$ of the incoming wavepacket, the yellow line is $V(t)$.

Figure 4. Transmitted charge through the constriction for the case of a linear voltage ramp, as a function of the ramp rate α and the offset V_0.

4.2. Step-like ramp

As mentioned in the introduction, performing the detection measurement with an energy-independent transmission probability that abruptly switches on or off allows one to measure the electron probability distribution as a function of time. Such an instantaneous switching on or off of the transmission function of the constriction requires an increase of the gate voltage $V(t)$ by an amount much larger than the energy uncertainty $\hbar/\sigma_t$ of the incoming wavepacket. Richer information about time and energy distribution can be obtained if the gate voltage jumps by a finite amount at time $t = t_0$,

$$V(t) = \begin{cases} V_i & \text{for } t < t_0, \\ V_f & \text{for } t > t_0. \end{cases} \tag{40}$$

For a Gaussian incoming wavepacket, the corresponding modified Wigner distribution can be calculated from equations (21) and (26),

$$\tilde{\rho}(E, t) = \frac{1}{\pi\hbar} e^{-2(E-E_0+V(t))^2\sigma_t^2/\hbar^2 - \frac{t^2}{2\sigma_t^2}} \operatorname{Re}\left\{ \operatorname{erf}\left[\frac{|t-t_0|}{\sqrt{2}\,\sigma_t} + \frac{i\sqrt{2}\,(E-E_0+V(t))\sigma_t}{\hbar} \right] \right\}$$

$$+ \frac{1}{\pi\hbar} \operatorname{Re}\left\{ e^{-2(E+\bar{V})^2\sigma_t^2/\hbar^2 - \frac{t^2}{2\sigma_t^2} - i(V_f-V_i)(t-t_0)/\hbar} \operatorname{erfc}\left[\frac{|t-t_0|}{\sqrt{2}\,\sigma_t} + \frac{i\sqrt{2}\,(E+\bar{V})}{\hbar} \right] \right\}, \tag{41}$$

Figure 5. Modified Wigner distribution in units of $1/\hbar$ of a Gaussian wave function after passing through a step-like ramp for different values of the barrier height $V_f - V_i$, compared to a non-transformed Wigner distribution (top left panel), as well as the semiclassical approximation (top right panel). We have set $V_i = E_0$ and $t_0 = 0$.

where we abbreviated

$$\bar{V} = \frac{1}{2}(V_f + V_i) - E_0. \tag{42}$$

A comparison between the initial-state Wigner function $\rho_{in}(E, t)$, the modified Wigner function $\tilde{\rho}(E, t)$ for two different parameter choices, and the semiclassical expectation[4] $\rho_{in}(E + V(t), t)$ is shown figure 5. Because of the abrupt time dependence at $t = t_0$, the semiclassical expectation is a poor approximation, as can be seen in the figure. In particular, the true modified distribution function is a continuous function of E and t, whereas the semiclassical expectation has a discontinuous jump by $V_f - V_i$ at $t = t_0$. The two lower panels of the figure show that in contrast to a linear ramp, a step-like ramp transforms the Wigner distribution such that it assumes negative values.

In figure 6 we show the transmitted charge at a fixed step height $V_f - V_i = 3\hbar/\sigma_t$ as a function of the center potential $\bar{V}$ and the switch time t_0. The top left panel shows the exact result (20), and the top right panel the semiclassical approximation (1). Their difference is shown in the bottom panel. As expected, if $|\bar{V}|$ is sufficiently large, the transmitted charge is independent of t_0 and approaches 0 or 1 (corresponding to maximum possible transmittance). For intermediate values of $\bar{V}$, there is a transition from 0 to 1 transmitted charge as t_0 goes from large negative to large positive values. Although the exact and the semiclassical results both reproduce the correct limits for large $|\bar{V}|$ and $|t_0|$, the behavior for small $\bar{V}$ and t_0 shows qualitative differences (such as shape of the median $Q = e/2$ curve), as well as quantitative differences (more than 0.1e, see bottom panel).

We can check explicitly that a large-amplitude sudden step in $V(t)$ will sample the time distribution. For this we need to prove that for $-V_i$, $V_f \gg \hbar/\sigma_t$, δ, finite E_0, and $\tilde{\rho}(E, t)$ given by equation (41), the transmitted charge

$$Q = \int_{-\infty}^{\infty} dE \int_{-\infty}^{\infty} dt \, T(E) \, \tilde{\rho}(E, t) \tag{43}$$

equals to $Q = \int_{-\infty}^{\infty} dE \int_{-\infty}^{t_0} dt \, \rho_{in}(E, t)$. Of the two terms in equation (41), the contribution of the second one to the time integral in equation (43) vanishes the limit of large $V_f - V_i$ due to fast oscillations, while the first term contributes only at $t < t_0$, when integrand is non-zero in the vicinity of $E \approx -V_i$. Taking the limit $V_i \to -\infty$, this gives

---

[4] We call $\rho_{in}(E + V(t), t)$ 'semiclassical' because it can be interpreted as a quasi-probability density for electrons that have a well-defined energy $E + V(t)$ at every time instant t.
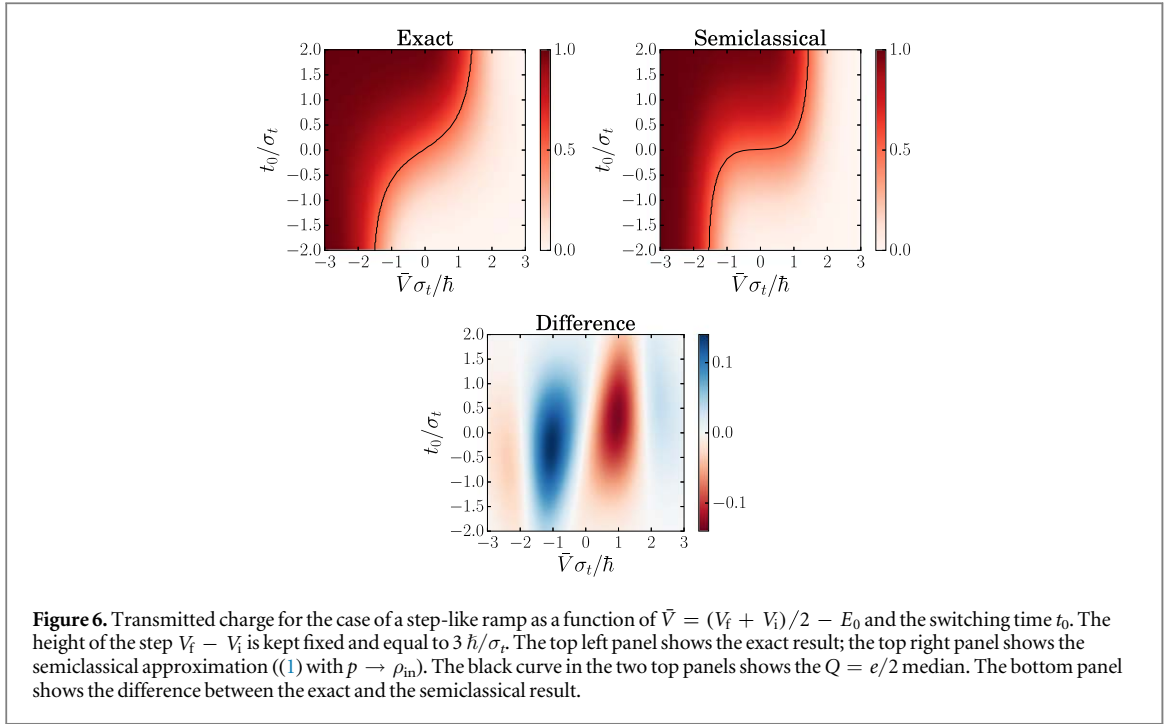
Figure 6. Transmitted charge for the case of a step-like ramp as a function of $\bar{V} = (V_f + V_i)/2 - E_0$ and the switching time t_0. The height of the step $V_f - V_i$ is kept fixed and equal to $3\,\hbar/\sigma_t$. The top left panel shows the exact result; the top right panel shows the semiclassical approximation ((1) with $p \rightarrow \rho_{in}$). The black curve in the two top panels shows the $Q = e/2$ median. The bottom panel shows the difference between the exact and the semiclassical result.

$$Q = \int_{-\infty}^{t_0} dt \int_{-\infty}^{\infty} dE' \rho_{in}(E', t)\{1 - \mathrm{Re}\, e^{z^2} w(z)]\}, \tag{44}$$

where $z = E'\sqrt{2}\,\sigma_t/\hbar + i(t_0 - t)/(\sqrt{2}\,\sigma_t)$ and $w(z)$ is Faddeeva function $w(z) = (i/\pi) \int e^{-\xi^2}/(z - \xi)\,d\xi$ ($\mathrm{Im}\, z > 0$). The first term in curly brackets in equation (44) gives the expected result. Straightforward integration confirms that the second term, proportional to $w(z)$, contributes zero.

4.3. Parabolic ramp

The third example is the case of a parabolic ramp, which may serve as an approximation of a periodic (sinusoidal) gate potential near the maximum or minimum of the potential. We consider a gate potential of the form

$$V(t) = V_0 - \frac{1}{2}W(t - t_0)^2. \tag{45}$$

The modified Wigner function is

$$\tilde{\rho}(E, t) = \frac{\sqrt{2/\pi}}{\sigma_t \sqrt[3]{|W|\,\hbar^2}} e^{-\frac{E - E_0 + V(t)}{W\sigma_t^2} - \frac{t^2}{2\sigma_t^2} + \frac{\hbar^2}{12W^2\sigma_t^6}}$$

$$\times \mathrm{Ai}\left[-\frac{2}{\sigma_t \sqrt[3]{W\hbar}}\left(E - E_0 + V(t) - \frac{\hbar}{8W\sigma_t^3}\right)\right], \tag{46}$$

where $\mathrm{Ai}(z)$ is the Airy function of the first kind.

Figure 7 contains a comparison between the exact result for the modified Wigner function, the semiclassical approximation (29) and a slow-potential approximation obtained by truncating the exponential in equation (31) at first order in the second derivative of the potential, for different values of W and for $V_0 = E_0 + \hbar/\sigma_t$, $t_0 = 0$. The figure confirms that both the semiclassical and the slow-potential approximation are good approximations for the modified Wigner function $\tilde{\rho}(E, t)$ if $|W| \ll \hbar/\sigma_t^3$, whereby the slow-potential approximation also faithfully reproduces some of the fringes at larger values of W, which are absent from the semiclassical approximation.

In figure 8 we show the transmitted charge for two different values of the the curvature parameter W, with separate panels for the exact result, the semiclassical approximation, and the slow-potential approximation. Their difference is shown in the bottom panels. The transmitted charge goes from zero for values of $V_0 - E_0$ far below the line $V_0 - E_0 = \frac{1}{2}Wt_0^2$ to 1 for values of $V_0 - E_0$ far above this line. The differences between the exact and the slow-potential solution grows with W, remaining below 1% for $W = 0.2\hbar/\sigma_t^3$ and going up to 10% for $W = 2\hbar\sigma_t^2$.
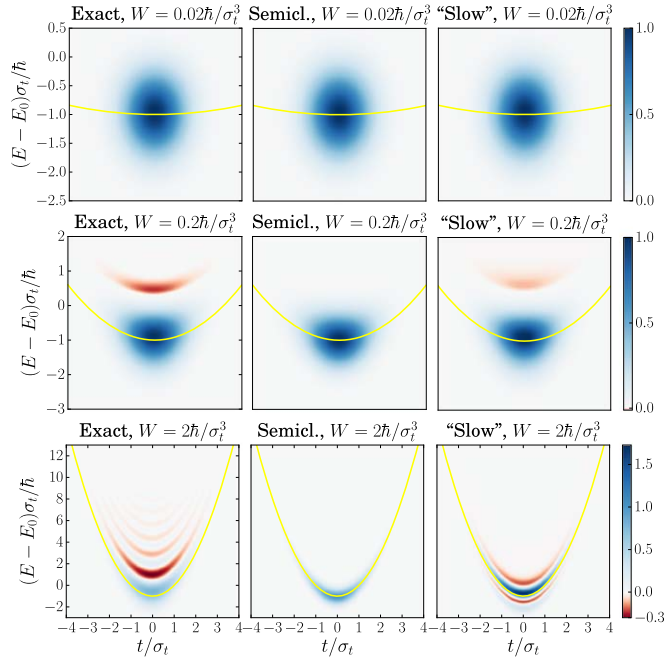
Figure 7. Modified Wigner distribution $\tilde{\rho}$ in units of $1/\hbar$ for a Gaussian wavepacket incident on the constriction. The gate potential $V(t)$ is taken to have the parabolic time dependence (45) with $W = 0.02\hbar/\sigma_t^3$ (top), $W = 0.2\hbar/\sigma_t^3$ (center), and $W = 2\hbar/\sigma_t^3$ (bottom). We have set $V_0 = E_0 + \hbar/\sigma_t$ and $t_0 = 0$. The left column shows the full quantum-mechanical result (20), the center column shows the semiclassical approximation (29), and right column shows the slow-potential approximation, obtained by truncating the exponential in equation (31) at first order in W.
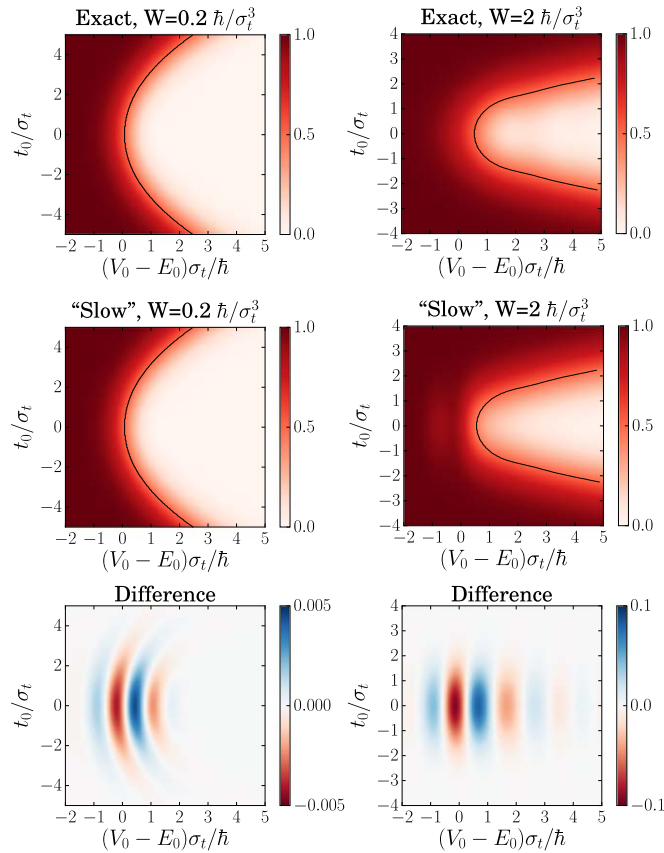

Figure 8. Transmitted charge Q for a Gaussian wavepacket incident on a constriction subject to a gate potential with the parabolic time dependence (45) with $W = 0.2\hbar/\sigma_t^3$ (left) and $W = 2\hbar/\sigma_t^3$ (right). The top row is obtained from the full quantum-mechanical expression equation (20), the center row uses the slow-potential approximation (31) with the exponential truncated after first order in the second derivative of the potential. The bottom row shows the difference between the slow-potential approximation and the full quantum-mechanical result.

5. Extension to non-chiral scattering

The results of section 3 and the examples discussed so far are exact for the model defined in section 2 which includes a strict separation of the scattering and the acceleration/deceleration regions, as well as linear dispersion. Here we demonstrate that our main results are robust against relaxing these assumptions, and show that equations (20)–(22) can provide a rather accurate approximation for scattering by a time-dependent one-dimensional potential controlled by a single gate even in the absence of a back-scattering-suppressing magnetic field.

In this section we compare analytical results of section 3 to a direct numerical solution of the time-dependent Schrödinger equation for the following Hamiltonian:

$$\hat{H}_{1D} = -\frac{\hbar^2}{2m^*}\frac{\partial^2}{\partial x^2} + V_c\, u(x) + V(t)u(x), \tag{47}$$

$$u(x) = \frac{1}{1 + \exp[(x - L_g/2)/l_g]} - \frac{1}{1 + \exp[(x + L_g/2)/l_g]}. \tag{48}$$

The second term and the third terms in equation (47) mimic the constriction part $\hat{H}_{bs}$ and the gate part $V(x, t) = V(t)u(x)$ of the Hamiltonian (2), respectively. For $L_g \gg l_g$ the potential form factor $u(x)$ is a mesa of height 1 with a flat plateaus part for $-L_g/2 < x < +L_g/2$, and rounded edges of characteristic width l_g (see figure 9(a)). This approximates the condition of spatially flat modulation. In the absence of modulation, $V(t) = 0$, the barrier height V_c determines the transmission energy threshold. We emphasize that (47) defines a model different to that of section 2, because both potential terms contribute to back-scattering between the left- and the right-movers; an approximate equivalence is expected only if $|V(t)| \ll V_c$ during scattering. In the comparison below, we consider linear modulation only, $V(t) = V_0 + \alpha\, t$ as in section 4.1, see equation (38).

For the numerical solution, the *x*-coordinate is discretised on a regular mesh with lattice spacing a and total number of sites $N \approx 16000$, the Hamiltonian (47) is approximated by a nearest-neighbor tight-binding Hamiltonian with hopping amplitude $-J$. The latter is fixed by matching the parabolic approximation at the bottom of the tight-binding band to the kinetic energy part of equation (47), i.e. $E(k) = 2J(1 - \cos ka) = \hbar^2 k^2/(2m^*) + O(k^4 a^4)$. Units of energy, length, and time are fixed by setting $J = 1, a = 1$ and $\hbar = 1$, which gives $m^* = 1/2$.

We follow propagation of the Gaussian wave-packet

$$\psi_0(x) \propto e^{ik_0 x}e^{-(\delta k)^2 x^2}, \tag{49}$$

which corresponds to approximately normal energy distribution of width $\sigma_E = \hbar^2 k_0\, \delta k/m^*$ centered at $E(k_0)$.

Split-step Fourier method [44, 45] is used to implement time evolution generated by $\hat{H}_{1D}(t)$. The initial state $\psi_{in}(x, t_0) = e^{+i\hat{H}_0 t_0}\psi_0(x)$, where $\hat{H}_0 = -\hbar^2(\partial/\partial x)^2/(2m^*)$, and time $t_0 < 0$ are chosen such that $\psi_{in}(x, t_0)$ is centred at least 10 standard deviations from the edge $\tilde{x}_g = -L_g/2$. This initial wave-packet is the propagated with full $\hat{H}_{1D}(t)$ from $t = t_0$ up to time $t = +1.5|t_0|$, and the transmitted fraction is computed by projecting the final state wave-function onto the subspace of right-movers (wave numbers $0 < k < \pi/(2a)$).

We set the working point for comparison to the linearised model at $V_c = E(k_c)$ with $k_c a = 0.25$ chosen so that the tight-binding approximation of the parabolic dispersion remains sufficiently accurate while the corresponding $E(k_c) = 0.062$ is large enough to explore the regime $|V_0|, \sigma_E \ll V_c$.

The numerical correspondence between the Gaussian wave-packets in the two models, equations (35) and (49), respectively, is established by $\psi_0(x) = \varphi_{in}(-x/v)e^{+ik_0 x - iE_0 x/(\hbar v)} \approx \varphi_{in}(-x/v)e^{ik_c x}$, with the velocity $v = \hbar^{-1}\partial E(k)/\partial k|_{k=k_c} \approx \hbar k_c/m^* = 0.5$ and the widths relation $\sigma_t\, \sigma_E = \hbar/2$. Here $e^{ik_c x}$ the carrier plane wave for which the amplitude distribution $\psi(x, t)$ (equation (7)) in the linearized model (2) acts as an envelope. Changing k_0 around k_c in equation (49) corresponds to changing $E_0 = E(k_0) - E(k_c) \approx \hbar v(k_0 - k_c)$ around 0 in equation (35).

The modified Wigner function (39) for the Gaussian incoming wave packet (35) and linear modulation (48), can be used to compute the transmitted charge from our general expression (20). Taking into account that $\mathcal{V}(t) = V_0 - \alpha L_g/(2v) + \alpha t$ for $u(x)$ given by equation (48) (computed in the limit $l_g \ll L_g$ with $x_b = 0$ and $x_g \to +\infty$ in equation (25); corresponds to the effective gate edge position $\tilde{x}_g = -L_g/2$ in contrast to $\tilde{x}_g = 0$ and $\mathcal{V}(t) = V(t)$ used in equation (39)), the extrapolation of our analytic theory to the one-dimensional model defined by $\hat{H}_{1D}$ reads

$$Q/e = \frac{1}{\tilde{\sigma}_E\sqrt{2\pi}}\int e^{-[E - E(k_0) + V_0 - \alpha L_g/(2v)]^2/(2\tilde{\sigma}_E^2)}T(E)\,\mathrm{d}E, \tag{50}$$

where $\tilde{\sigma}_E = \sqrt{\sigma_E^2 + \hbar^2\alpha^2/(4\sigma_E^2)}$. Equation (50) includes the transmission probability $T(E)$ for the static potential $V_c\, u(x)$; we compute $T(E)$ numerically using the scattering matrix expression in terms of a numerically computed Green function as in [46].
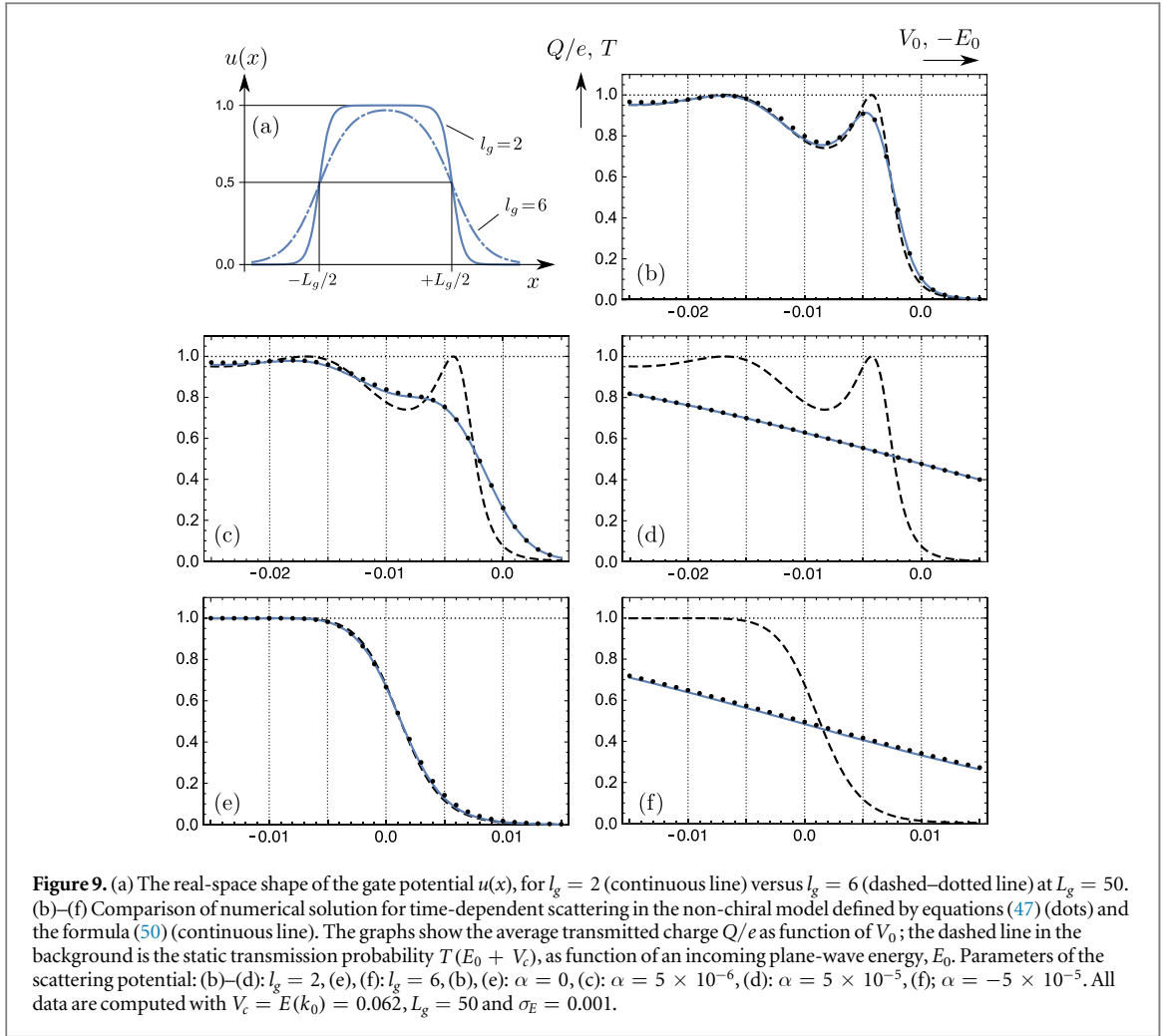
Figure 9. (a) The real-space shape of the gate potential $u(x)$, for $l_g = 2$ (continuous line) versus $l_g = 6$ (dashed–dotted line) at $L_g = 50$. (b)–(f) Comparison of numerical solution for time-dependent scattering in the non-chiral model defined by equations (47) (dots) and the formula (50) (continuous line). The graphs show the average transmitted charge Q/e as function of V_0; the dashed line in the background is the static transmission probability $T(E_0 + V_c)$, as function of an incoming plane-wave energy, E_0. Parameters of the scattering potential: (b)–(d): $l_g = 2$, (e), (f): $l_g = 6$, (b), (e): $\alpha = 0$, (c): $\alpha = 5 \times 10^{-6}$, (d): $\alpha = 5 \times 10^{-5}$, (f); $\alpha = -5 \times 10^{-5}$. All data are computed with $V_c = E(k_0) = 0.062$, $L_g = 50$ and $\sigma_E = 0.001$.

Figures 9(b)–(f) plot the probability of transmission Q/e for the same initial wave packet ($k_0 = k_c$ and $\sigma_E = 10^{-3}$), but different sharpness ($l_g = 2$ versus $l_g = 6$) and modulation speed ($\alpha = 0, 5 \times 10^{-6}$, and $\pm 5 \times 10^{-5}$) of the barrier, as function of the additional barrier height V_0. We note rather accurate agreement between the direct numerical integration (dots) and the approximation (50) (continuous blue line), validating the main thesis of this section.

Additionally, we plot the transmission $T(E)$ as function of energy (dashed line). For small $\tilde\sigma_E$, see figures 9(b), (e), the transmitted charge follows $T(E)$ since Since (50) is a convolution of $T(E)$ and a Gaussian function of width $\tilde\sigma_E$, the transmitted charge follows $T(E)$. Note that this agreement is a direct demonstration of the relation $T(E_0, V_0) = T(E_0 - V_0)$ for the potential shown in figures 9(a) because T is computed by varying E_0, and Q is computed by varying V_0.

The sharper shape of $T(E)$ in figures 9(b)–(d) corresponds to a steeper potential edge ($l_g = 2$) compared to a wider step-like $T(E)$ for $l_g = 6$ in figures 9(e), (f). Transmission maxima arise due to multiple-reflection resonances at quasi-bound state energies $E_0 = \pi^2\hbar^2 n^2/(2m^*L_g^2)$ where $n = 1, 2\ldots$ is the number of halfwavelengths matching the distance between sharp edges L_g. We note that by increasing L_g and adjusting the rounding parameter $l_g(L_g) \ll L_g$ accordingly, one can achieve a smooth transition from $T = 0$ to $T = 1$ over an arbitrarily narrow energy range, suitable for modified Wigner function filtering as assumed in the examples of section 4 and discussed in the context of the tomography technique below in section 6.

We conclude the discussion of the one-dimensional model (47) with an example of potential parameters at which the analytic result (49) borrowed from the chiral model with local backscattering (section 2) clearly fails. If the barrier is too thin, tunnelling across the full width of the barrier becomes relevant, the scattering is not localized at the edges, and adjusting of the barrier height can no longer be approximated by a uniform shift in energy. For an unmodulated ($\alpha = 0$) rectangular ($l_g \to 0$), barrier of height V the exact subthreshold ($E < V$) transmission is $T_{\text{rect}}(E, V) = \{1 + V^2 \sinh^2[L_g\sqrt{2m(V - E)}/\hbar]/[4E(V - E)]\}^{-1}$. If $L_g \gg \hbar/\sqrt{2mV_c} \approx 4.0$ (for the parameter values used in figure 9), the product $(V_c + E_0)(V_0 - E_0)$ in $T(V_c + E_0, V_c + V_0)$ is well-approximated by $V_c(V_0 - E_0)$ and T is a function of $E_0 - V_0$ only, as in the numerical examples above. For $L_g = 5$, however, the approximation breaks down as a numerical calculation
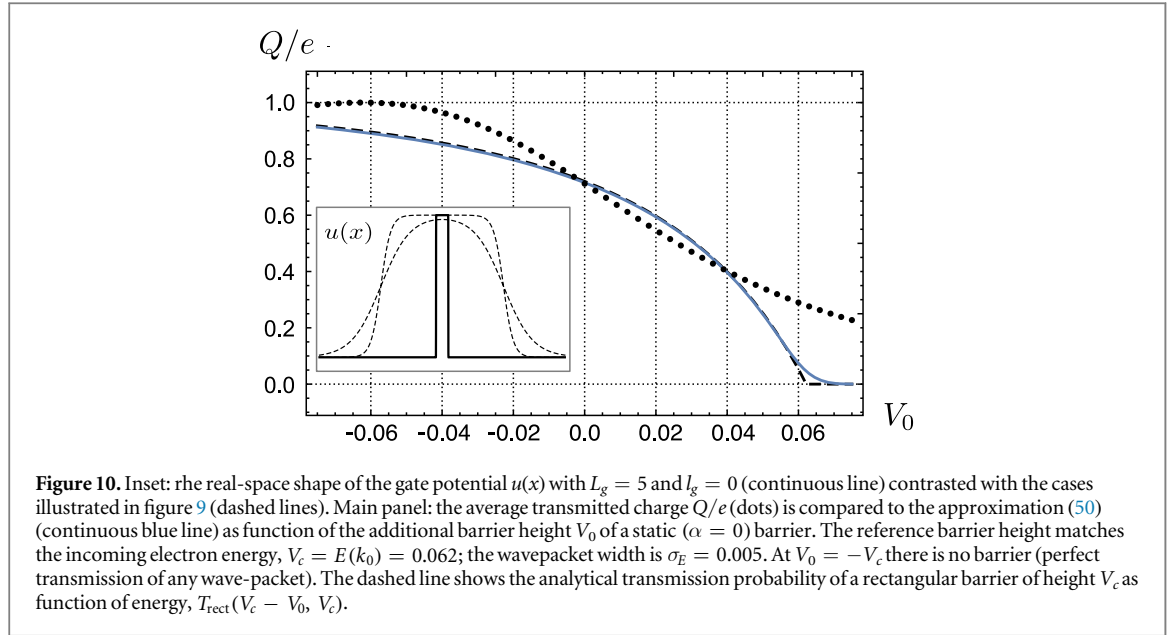
Figure 10. Inset: rhe real-space shape of the gate potential $u(x)$ with $L_g = 5$ and $l_g = 0$ (continuous line) contrasted with the cases illustrated in figure 9 (dashed lines). Main panel: the average transmitted charge Q/e (dots) is compared to the approximation (50) (continuous blue line) as function of the additional barrier height V_0 of a static ($\alpha = 0$) barrier. The reference barrier height matches the incoming electron energy, $V_c = E(k_0) = 0.062$; the wavepacket width is $\sigma_E = 0.005$. At $V_0 = -V_c$ there is no barrier (perfect transmission of any wave-packet). The dashed line shows the analytical transmission probability of a rectangular barrier of height V_c as function of energy, $T_{\rm rect}(V_c - V_0, V_c)$.

shown in figure 10 illustrates. In this example, equation (49) uses $T(E) = T_{\rm rect}(E, V_c)$ (computed numerically in the tight-binding approximation), which thus must agree with the direct wave-packet propagation approach at $V_0 = 0$, as indeed is the case in figure 10. However, as V_0 is varied, the scattering of the wave-packets incoming at $E(k_0) = V_c$ is no longer equivalent to wavepackets impinging at an unmodified ($V_0 = 0$) barrier at an energy $E(k_0) = V_c - V_0$.

6. Connection to experiment

In this section we discuss the relevance of our results to the recently proposed and implemented tomography protocol for solitary electrons [40].
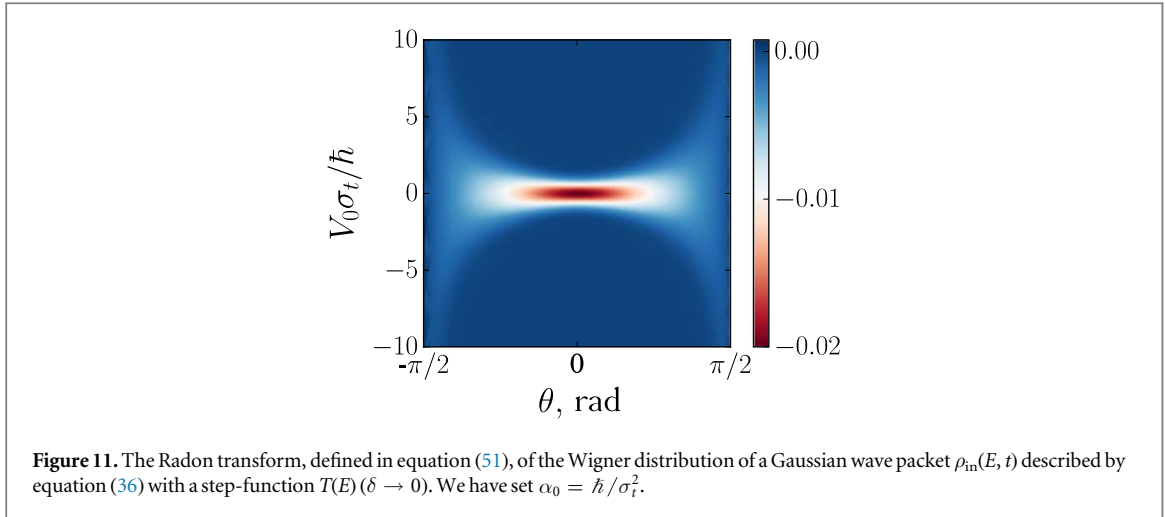
6.1. Scattering by a linearly modulated barrier as a Radon transform

As mentioned in the introduction, the tomography experiment provides a map of the charge $Q(V_0, \alpha)$ transmitted through barrier that is controled by a gate voltage $V(t) = \alpha t + V_0$ with a linear time dependence as a function of the energy offset V_0 and the energy-time slope $\alpha = \alpha_0 \tan \theta$, where α_0 is a scale factor adapted to the characteristic time and energy scales of the experiment. The quantity

$$e^{-1}\frac{\partial Q(V_0, \theta)}{\partial V_0} = \int \mathrm{d}t \; \mathrm{d}E \frac{\partial T(E - V_0 - \alpha_0 \, t \tan \theta)}{\partial V_0}\rho_{\rm in}(E, t)$$

$$= \int \mathrm{d}t \int \mathrm{d}E \; \frac{\mathrm{d}T(E)}{\mathrm{d}E} \, \rho_{\rm in}(V_0 + \alpha_0 \, t \tan \theta - E, t) \tag{51}$$

represents the Radon transform [47] of the incoming Wigner distribution $\rho_{\rm in}(E, t)$ convolved with the energy derivative of the transmission coefficient $\mathrm{d}T/\mathrm{d}E$. In equation (51) we have used the fact that, according to equation (29), for a linear ramp the modified Wigner function $\tilde{\rho}(E, t)$ can be expressed in terms of the incoming Wigner function $\rho_{\rm in}(E, t)$ simply by adding $V(t)$ to the energy. The tomography protocol of [40] consists of measuring (51) for a sufficiently wide range of V_0 and θ to enable numerical computation of the the inverse Radon transform using the standard filtered back-projection algorithm [47]. A sufficiently sharp $T(E)$, such that the derivative $\mathrm{d}T/\mathrm{d}E$ can be approximated as a delta function, ensures that the inversion accurately represents the unknown $\rho_{\rm in}(E, t)$.

To illustrate the Radon transform, in figure 11 we have shown the quantity $\partial Q(V_0, \theta)/\partial V_0$ calculated for the incoming Wigner distribution $\rho_{\rm in}(E, t)$ of a Gaussian wave packet, exactly like the one depicted in the top left panel of figure 3. The Radon transform is the line integral of $\rho_{\rm in}(E, t)$ along the straight line $E = V_0 + \alpha_0 t \tan \theta$. The non-zero values in figure 11 are concentrated around $\theta = 0$. A correlation between energy and time [42] that has a slope β in the time-energy plane would introduce a shift by $\arctan(\beta/\alpha_0)$ along the θ axis [40]. Notice that the width of the non-zero regions along the V_0 axis at $\theta = 0$ corresponds to the quantum-limited energy width $\hbar/(2\sigma_t)$ of the Gaussian distribution, as $\delta \to 0$ in this example.

Figure 11. The Radon transform, defined in equation (51), of the Wigner distribution of a Gaussian wave packet $\rho_{in}(E, t)$ described by equation (36) with a step-function $T(E)$ ($\delta \to 0$). We have set $\alpha_0 = \hbar / \sigma_t^2$.

6.2. Resolution limits

A finite sharpness δ of the transmission function $T(E)$ in equation (51) can be seen as a finite resolution of the measurement apparatus that defines the energy level against which $\rho_{in}(E, t)$ is inferred by the tomography protocol. For $dT(E)/dE \geqslant 0$, the convolution of the incoming Wigner function $\rho_{in}(E, t)$ with $\partial T/\partial E$ in (51) can be interpreted as the Wigner representation

$$\rho_{eff}(E, t) = (\pi \hbar)^{-1} \int e^{i2E\, t'/\hbar} \langle t + t'| \hat{\rho}|t - t'\rangle \, dt \tag{52}$$

of an effective density matrix

$$\langle t|\hat{\rho}|t'\rangle = \int dE \frac{dT(E)}{dE} \varphi_E(t) \varphi_E^*(t') \tag{53}$$

$$= \varphi_{in}(t)\, \Pi(t - t')\, \varphi_{in}^*(t'), \tag{54}$$

where $\varphi_E(t) = \varphi_{in}(t)e^{-iEt/\hbar}$ is the incoming state $\varphi_{in}(t)$ shifted in energy by E, and $\Pi(t) = \int e^{-iEt/\hbar} dT(E)$. In the limit of $\delta \to 0$, dT/dE becomes a delta-function, $\Pi(t - t')$ becomes 1, and $\rho_{eff}(E, t)$ in equation (52) reduces to the pure-state Wigner function (10). For finite δ though, the characteristic temporal width $\hbar/\delta$ of the Fourier transform $\Pi(t - t')$ in the time-domain representation (equation (54)) sets the upper limit on the coherence time of the wave-packet that can be resolved by the tomographic reconstruction.

For $\delta > 0$, electron partitioning at the barrier introduces shot noise that reduces the purity of the reconstructed effective mixed state $\hat{\rho}$. We illustrate this by computing the convolution of the uncorrelated Gaussian wavepacket (35) and a Gaussian dT/dE from equation (37),

$$\rho_{eff}(E, t) = \frac{1}{2\pi\sqrt{(\hbar/2)^2 + (\sigma_t\, \delta)^2}} \exp\left\{ -\frac{t^2}{2\sigma_t^2} - \frac{1}{2} \frac{(E - E_0)^2}{[\hbar/(2\sigma_t)]^2 + \delta^2} \right\}. \tag{55}$$

Quantum purity, defined as $\gamma = \text{tr}\rho^2$, is straightforward to compute in the Wigner representation, $\gamma = h \iint \rho_{eff}(E, t)\, dE\, dt$ [40]. Using (55) we obtain the effective purity of tomographic reconstruction by a finite-width barrier for a quantum-limited Gaussian wave-packet,

$$\gamma = \frac{\hbar/2}{\sqrt{(\hbar/2)^2 + (\sigma_t\, \delta)^2}}. \tag{56}$$

We see that γ in the case of an uncorrelated Gaussian wavepacket is equal to the ratio between the ideal Heisenberg uncertainty product ($\hbar/2$) and the product of time and energy widths in the effective distribution (55) which is broadened by a finite resolution δ of the energy detector. Note that in general, the uncertainty product alone is insufficient to distinguish the incoherent broadening (e.g. δ-dependent terms in equation (55)) from coherent broadening (e.g. the energy-time correlation created in the source [40, 42]). Hence a full tomography technique is essential for evaluating the quality a source with respect to the quantum limit of localizing a single particle in energy and time.

The dependence of δ on the parameters of the constriction depends on the details of the scattering interaction $\hat{H}_{bs}$ and goes beyong the scope of this work. Nevertheless, we can use the simple sketch in figure 2 for an order of magnitude estimate. For a single-channel model with the backscattering amplitude distributed spatially over a length $x \in [-x_b \ldots + x_b]$, the temporal width of $\tau(t)$ (and hence $\Pi(t)$) is limited by $2 x_b/v$. This gives an estimate

$$\delta \gtrsim \frac{\hbar v}{x_b} \tag{57}$$

for the achievable energy resolution of the tomography technique within a specific model of the scattering barrier depicted schematically in figure 2. This bound can also be interpreted as $x_b \, \Delta p \gtrsim \hbar$ where $\Delta p = \delta/v$ is the Fourier (diffraction) limit on the momentum resolution achievable over the characteristic length x_b of the backscattering region for a particle propagating with velocity v.

One can expect from equation (57) that the effective length of the spatially uniform part of the scattering region is an important parameter for designing a barrier suitable for high-resolution tomography. On the other hand, as we have seen in section 3.2, the length and the shape of the gate edge region from $-x_g$ to $-x_b$ is not important as long as the linear-in-time modulation condition (27) is fulfilled and the velocity dispersion can be ignored.

6.3. Measurement of the modified Wigner function

As mentioned in section 3, the modified Wigner function $\tilde{\rho}(E, \, t)$ is not a physical observable and does not represent the Wigner function of the wave packet at any stage. However, it can be experimentally obtained as the outcome of tomographic reconstruction. To see this, we consider a gate voltage $V(t)$ that is the sum of a linear part $V_0 + \alpha t$, as in the experiment of [40], and an additional perturbation $V'(t)$. This scenario is discussed theoretically at the end of section 3.2, see equations (33) and (34). Analogously to equation (51), the modified Wigner function corresponding to the perturbation $V'(t)$ only, can be expressed as

$$\frac{\partial Q(V_0, \, \theta)}{\partial V_0} = e \int dt \, \tilde{\rho}'(V_0 + \alpha_0 \, t \tan \theta, \, t), \tag{58}$$

where we have assumed ideal energy resolution, inserted $\mathcal{V}(t) = V_0 + \alpha_0 \, t \tan \theta$, and absorbed the correction to $V(t)$ due to a possibly non-sharp edge of the gate into V_0. This result means that, if we perform the inverse Radon transform of $\partial Q(V_0, \, \theta)/\partial V_0$, the outcome would be the modified Wigner distribution calculated for the non-linear part $V'(t)$ of the potential $V(t)$ only. For example, the function $\tilde{\rho}(E, \, t)$ of equation (41) can be measured using the linear tomographic reconstruction protocol of [40] while applying a gate voltage that is the sum of equations (38) and (40), i.e.

$$V(t) = \begin{cases} V_0 + \alpha t + V_i & \text{for } t < t_0, \\ V_0 + \alpha t + V_f & \text{for } t > t_0. \end{cases} \tag{59}$$

By introducing such a sharp voltage 'kick' on top of a linear time dependence of the gate potential, it would be possible to gather direct evidence of coherence of the electron source, since negative values in the measurement of $\tilde{\rho}'(E, \, t)$ arise from interference between phase-coherent parts of the incoming wave packet. This is relevant for the investigation of the properties of single-electron sources that emit solitary electrons high above the Fermi energy, where coherence is key to potential interferometric applications [3].

Our results also provide a way to describe a different kind of problem: sampling the potential $V(t)$ with single electrons whose incoming distribution is well known [48]. In this case, the deviations in the measurement of $\rho_{in}(E, \, t)$ from the actual incoming distribution may allow one to measure the wave-form $V(t)$ beyond the classical resolution limit. In this context, equation (25) can elucidate the influence of the potential shape on the bandwidth of such a 'quantum oscilloscopic' measurement.

7. Conclusions

Inspired by recent experiments [39, 40], we have constructed a fully quantum-mechanical description of a dynamical scattering problem of electron wave packets in a one-dimensional chiral channel passing through a constriction subject to a time-dependent gate potential $V(t)$. We have shown that the expression for the transmitted charge in this system is analogous to the corresponding classical expression, with a modified Wigner distribution function $\tilde{\rho}$ being the quantum analog of the classical probability distribution. In particular, if the gate voltage time dependence is linear then the modified Wigner distribution is obtained from the Wigner function of the incoming electron by a time-dependent shift of the energy E. In this case the full quantum-mechanical theory agrees with the classical-limit estimate (1) justifying the quantum tomography proposal put forward in [40].

A finite energy resolution δ of the scattering barrier adds shot noise to the tomographically reconstructed Wigner distribution, limiting the maximal coherence time that can be probed by $\hbar/\delta$. Small δ requires large spatial extent x_b of the uniformly modulated part of the constriction, $\delta \geqslant \hbar v/x_b$. We have shown that neither the length of the wave-packet nor the shape of the accelerating edge of the gate potential perturbs the linear tomography protocol as long as the modulation of the scattering region remains spatially uniform.

Our fully quantum-mechanical theory provides the tools to analyze experiments with a general time dependence of the gate voltage, relevant for wave-packets that are stretched in the time domain. The results presented here can be used to describe existing and propose new quantum measurement protocols. They can also serve to analyze a reverse problem: determining the gate potential $V(t)$ when the incoming electron distribution is known. We have shown that additional modification of the Wigner function by non-linear gate modulation can in principle be revealed by quantum tomography within the same device. This opens a possibility to probe coherence of single-electron sources with explicit signatures of quantum interference (e.g. negativity of the modified Wigner function) which does not require multiple-path layouts.

Acknowledgments

ORCID iDs

Vyacheslavs Kashcheyevs ● https://orcid.org/0000-0002-4869-8837

References

[1] Grenier C, Hervé R, Fève G and Degiovanni P 2011 *Mod. Phys. Lett.* B **25** 1053
[2] Bocquillon E *et al* 2014 *Ann. Phys.* **526** 1
[3] Bäuerle C, Glattli C, Meunier T, Portier F, Roche P, Roulleau P, Takada S and Waintal X 2018 *Rep. Prog. Phys.* **81** 056503
[4] Marguerite A, Bocquillon E, Berroir J-M, Plaçais B, Cavanna A, Jin Y, Degiovanni P and Fève G 2017 *Phys. Status Solidi* B **254** 1600618
[5] Roussel B, Cabart C, Fève G, Thibierge E and Degiovanni P 2017 *Phys. Status Solidi* B **254** 1600621
[6] Demkowicz-Dobrzański R, Kołodyński J and Guţă M 2012 *Nat. Commun.* **3** 1063
[7] Pothier H, Lafarge P, Urbina C, Esteve D and Devoret M H 1992 *Europhys. Lett.* **17** 249
[8] Switkes M, Marcus C M, Campman K and Gossard A C 1999 *Science* **283** 1905
[9] Fève G, Mahé A, Berroir J-M, Kontos T, Plaçais B, Glattli D C, Cavanna A, Etienne B and Jin Y 2007 *Science* **316** 1169
[10] Blumenthal M D, Kaestner B, Li L, Giblin S, Janssen T J B M, Pepper M, Anderson D, Jones G and Ritchie D A 2007 *Nat. Phys.* **3** 343
[11] Fujiwara A, Nishiguchi K and Ono Y 2008 *Appl. Phys. Lett.* **92** 042102
[12] Pekola J P, Vartiainen J J, Möttönen M, Saira O-P, Meschke M and Averin D V 2008 *Nat. Phys.* **4** 120
[13] Kaestner B *et al* 2008 *Phys. Rev.* B **77** 153301
[14] Wright S J *et al* 2008 *Phys. Rev.* B **78** 233311
[15] Kaestner B, Leicht C, Kashcheyevs V, Pierz K, Siegner U and Schumacher H W 2009 *Appl. Phys. Lett.* **94** 012106
[16] Chorley S J, Frake J, Smith C G, Jones G A C and Buitelaar M R 2012 *Appl. Phys. Lett.* **100** 143104
[17] Connolly M R *et al* 2013 *Nat. Nanotechnol.* **8** 417
[18] Dubois J, Jullien T, Grenier C, Degiovanni P, Roulleau P and Glattli D C 2013 *Phys. Rev.* B **88** 085301
[19] Ubbelohde N, Hohls F, Kashcheyevs V, Wagner T, Fricke L, Kästner B, Pierz K, Schumacher H W and Haug R J 2015 *Nat. Nanotechnol.* **10** 46
[20] d'Hollosy S, Jung M, Baumgartner A, Guzenko V A, Madsen M H, NygÅrd J and Schönenberger C 2015 *Nano Lett.* **15** 4585
[21] Roussely G *et al* 2018 *Nat. Commun.* **9** 2811
[22] Henny M, Oberholzer S, Strunk C, Heinzel T, Ensslin K, Holland M and Schönenberger C 1999 *Science* **284** 296
[23] Oliver W D, Kim J, Liu R C and Yamamoto Y 1999 *Science* **284** 299
[24] Kiesel H, Renz A and Hasselbach F 2002 *Nature* **418** 392
[25] Bocquillon E, Parmentier F D, Grenier C, Berroir J-M, Degiovanni P, Glattli D C, Plaçais B, Cavanna A, Jin Y and Fève G 2012 *Phys. Rev. Lett.* **108** 196803
[26] Bocquillon E, Freulon V, Berroir J-M, Degiovanni P, Plaçais B, Cavanna A, Jin Y and Fève G 2013 *Science* **339** 1054
[27] Ferraro D, Ronetti F, Vannucci L, Acciai M, Rech J, Jockheere T, Martin T and Sassetti M 2018 *Eur. Phys. J. Spec. Top.* **227** 1345
[28] Ji Y, Chung Y, Sprinzak D, Heiblum M, Mahalu D and Shtrikman H 2003 *Nature* **422** 415
[29] Neder I, Heiblum M, Levinson Y, Mahalu D and Umansky V 2006 *Phys. Rev. Lett.* **96** 016804
[30] Neder I, Heiblum M, Mahalu D and Umansky V 2007 *Phys. Rev. Lett.* **98** 036803
[31] Bocquillon E *et al* 2014 *Ann. Phys.* **526** 1
[32] Grenier C, Hervé R, Bocquillon E, Parmentier F D, Plaçais B, Berroir J M, Fève G and Degiovanni P 2011 *New J. Phys.* **13** 093007
[33] Jullien T, Roulleau P, Roche B, Cavanna A, Jin Y and Glattli D C 2014 *Nature* **514** 603
[34] Bisognin R *et al* 2019 Extracting single electron wavefunctions from a quantum electrical current *Nat. Commun.* **10** 3379
[35] Leicht C, Mirovsky P, Kaestner B, Hohls F, Kashcheyevs V, Kurganova E V, Zeitler U, Weimann T, Pierz K and Schumacher H W 2011 *Semicond. Sci. Technol.* **26** 055010
[36] Fletcher J D *et al* 2013 *Phys. Rev. Lett.* **111** 216807
[37] Waldie J, See P, Kashcheyevs V, Griffiths J P, Farrer I, Jones G A C, Ritchie D A, Janssen T J B M and Kataoka M 2015 *Phys. Rev.* B **92** 125305

[38] Kataoka M, Johnson N, Emary C, See P, Griffiths J P, Jones G A C, Farrer I, Ritchie D A, Pepper M and Janssen T J B M 2016 *Phys. Rev. Lett.* **116** 126803

[39] Kataoka M, Fletcher J D and Johnson N 2017 *Phys. Status Solidi* B **254** 1600547

[40] Fletcher J D, Johnson N, Locane E, See P, Griffiths J P, Farrer I, Ritchie D A, Brouwer P W, Kashcheyevs V and Kataoka M 2019 Continuous-variable tomography of solitary electrons *Nat. Commun.* arXiv:1901.10985

[41] Ferraro D, Feller A, Ghibaudo A, Thibierge E, Bocquillon E, Fève G, Grenier C and Degiovanni P 2013 *Phys. Rev.* B **88** 205303

[42] Kashcheyevs V and Samuelsson P 2017 *Phys. Rev.* B **95** 245424

[43] Emary C, Clark L A, Kataoka M and Johnson N 2019 *Phys. Rev.* B **99** 045306

[44] Feit M, Fleck J and Steiger A 1982 *J. Comput. Phys.* **47** 412

[45] Bellentani L, Beggi A, Bordone P and Bertoni A 2018 *Phys. Rev.* B **97** 205419

[46] Aharony A and Entin-Wohlman O 2002 *Phys. Rev.* B **65** 241401

[47] Deans S R 1983 *The Radon Transform and Some of Its Applications* (New York: Wiley)

[48] Johnson N *et al* 2017 *Appl. Phys. Lett.* **110** 102105